

Discrimination between Rain and Snow with a Polarimetric Radar

A. V. RYZHKOV

Cooperative Institute for Mesoscale Meteorological Studies, University of Oklahoma, Norman, Oklahoma

D. S. ZRNIC

National Severe Storms Laboratory, Norman, Oklahoma

(Manuscript received 28 October 1996, in final form 30 December 1997)

ABSTRACT

Polarimetric signatures of snow precipitation for six Oklahoma snowstorms are examined. The available data consist of specific differential phase K_{DP} , differential reflectivity Z_{DR} , cross-correlation coefficient ρ_{hv} , and radar reflectivity factor Z . These data were obtained with the 10-cm-wavelength Cimarron polarimetric weather radar. The data suggest that in pure snow the average values of K_{DP} and Z_{DR} do not follow a systematic trend with change of the radar reflectivity factor if $Z < 35$ dBZ; this is not the case in rain. Precipitation is qualified as snow if the average Z_{DR} is less than 0.2 dB for $Z < 35$ dBZ. The presence of a bright band with a pronounced ρ_{hv} minimum and Z_{DR} maximum is a good discernible feature for discriminating between snow and rain. Thus, a localized deep minimum of the cross-correlation coefficient delineates the transition region between snow and rain in the horizontal direction if sufficiently large snowflakes are generated in the transition area. Otherwise, a sharp change of Z_{DR} can be used to localize the position of the snow–rain line.

1. Introduction

Remote delineation of the transition region between rain and snow is of great importance because these two precipitation types have vastly different yet significant social and economical impacts in the regions of occurrence. Forecasts of the expected location of rain–snow boundaries are somewhat elusive and often based on incomplete or inadequate climatological information. Knowledge of the exact location of the rain–snow boundary is also necessary to accurately determine the precipitation amounts. Currently there is no operational algorithm to gauge snow amounts from the WSR-88D radar network. The available relation $Z = 300R^{1.4}$ is used for rainfall estimation. On the basis of temperature, or snow reports, the operators manually adjust this relation to obtain the snowfall amounts (Gunn and Marshall 1958). Better methods to discriminate snow and quantify its amount can be applied to the reflectivity data and are being contemplated. Nevertheless, the need to know the type of precipitation before determining the amount puts a fundamental limitation to what the reflectivity factor can offer.

A natural way to discriminate between snow and rain is to look for a region of enhanced reflectivity associated

with melting snow, that is, the so-called bright band (Martner et al. 1993). Presumably in the region below a bright band rainfall is occurring at the ground. However, long-term observations of the melting layer made by Fabry and Zawadzki (1995) show that low-level rain and rain developed from compact ice do not exhibit a bright band at all. Moreover, sometimes it is very difficult to identify the bright band using the radar reflectivity factor, especially at long ranges where the radar beam is much wider than the melting layer.

Radar polarimetry has proved useful to discriminate between liquid and solid hydrometeors and to localize zones of hail and graupel within severe convective storms. The radar reflectivity factor combined with differential reflectivity can be used to discriminate between rain and ice hydrometeors (Leitao and Watson 1984) as well as hail (Aydin et al. 1986). Specific differential phase also helps to identify precipitation type as rain, hail, and rain–hail mixture (Balakrishnan and Zrnic 1990). Hall et al. (1984) classified hydrometeors of different types (rain of various intensity, dry snow, ice crystals, aggregated snow, graupel, hail) according to their radar reflectivity, depolarization ratio, and magnitude of cross-correlation coefficient between orthogonal components of backscatter field. They considered measurements at circular polarization basis, however, and this type of classification has never been exploited in later studies. Part of the problem is that polarimetric signatures of meteorological scatterers are much more affected by propagation effects with a circular polar-

Corresponding author address: Dr. Alexander V. Ryzhkov, CIMMS, NOAA/NSSL, 1313 Halley Circle, Norman, OK 73069.
E-mail: ryzhkov@ruth.nssl.noaa.gov

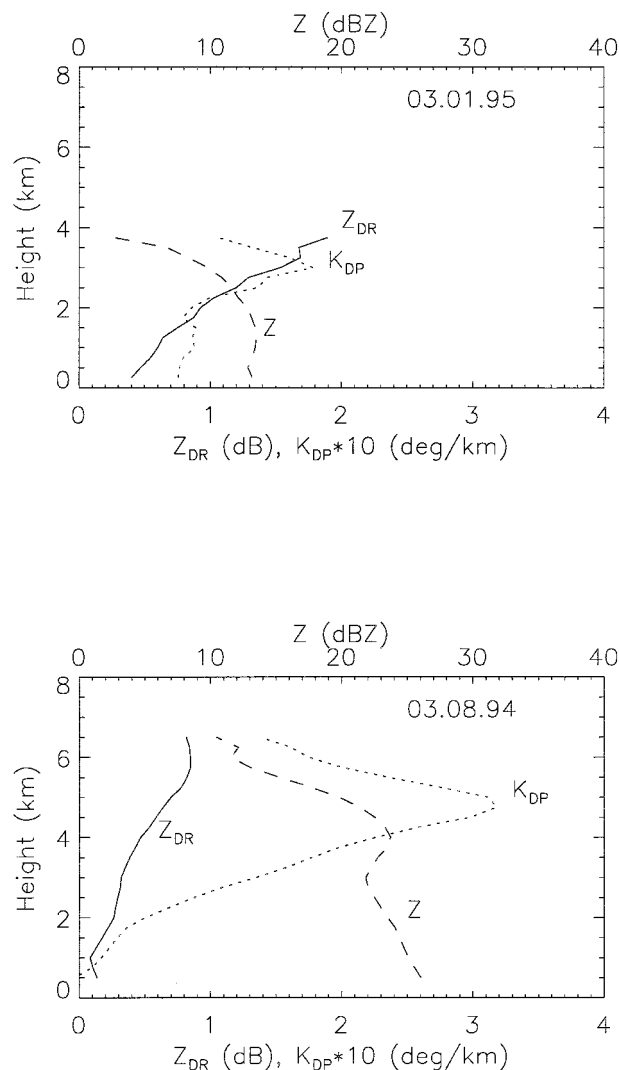


FIG. 1. Vertical profiles of Z , Z_{DR} , and K_{DP} for (a) "cold" and (b) "warm" snowfall.

ization basis than with a linear polarization basis that has gained favor for most applications on dual-polarization research radars.

There are three polarimetric variables in addition to conventional radar reflectivity factor Z that the Cimarron National Severe Storm Laboratory's 10-cm-wavelength polarimetric radar can provide. These variables are differential reflectivity Z_{DR} , specific differential phase K_{DP} , and cross-correlation coefficient ρ_{hv} . For pure rain media, polarimetric signatures have been well investigated to draw some definite conclusions. Both K_{DP} and Z_{DR} grow rapidly with the increasing reflectivity or rain intensity because the shape of raindrops becomes more oblate as the size increases. For snow a relation between shape and size is not well established. Bulk density of snowflakes is one more unknown that complicates interpretation. One can hypothesize that only small crystals with sizes less than 0.1 mm have bulk densities

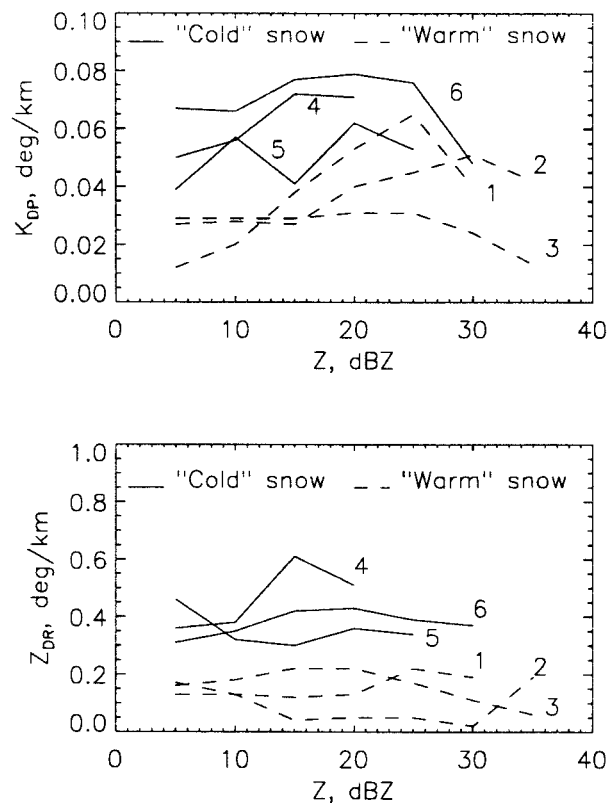


FIG. 2. The dependencies of average (a) K_{DP} and (b) Z_{DR} on Z for snow near the ground in six different snowstorms. The numbers next to the graphs denote the different storms as follows: 1, 8 Mar 1994; 2, 5 Jan 1995; 3, 18 Dec 1995; 4, 1 Mar 1995; 5, 2 Mar 1995; and 6, 1 Feb 1996.

close to that of a pure ice. Bigger snow particles, grown via aggregation, have densities inversely proportional to size (Brown and Francis 1995). Therefore, the radar reflectivity Z , as well as Z_{DR} and K_{DP} for snow particles, are expected to increase slower with size compared to raindrops. Larger snowflakes apparently are more likely to tumble and wobble during fall than small crystals, thus further decreasing Z_{DR} and K_{DP} . In other words, one would expect relatively small values of these two polarimetric parameters throughout the whole range of reflectivities in dry aggregated snow. The reflectivity of snow rarely exceeds 40 dBZ, and rain with similar reflectivities also produces low K_{DP} and Z_{DR} ; therefore, discrimination between pure snow and pure rain is not straightforward.

Snow can exhibit much more pronounced polarimetric signatures if (a) it consists mostly of small nonspherical well-oriented crystals and (b) it is melting. Ice crystals are the dominant scatterers at tops of mixed-phase clouds or even close to the ground if surface temperature is very low and aggregation is not pronounced. Ice crystals produce an order of magnitude larger differential reflectivity Z_{DR} and specific differential phase K_{DP} than dry aggregated snow (Meischner

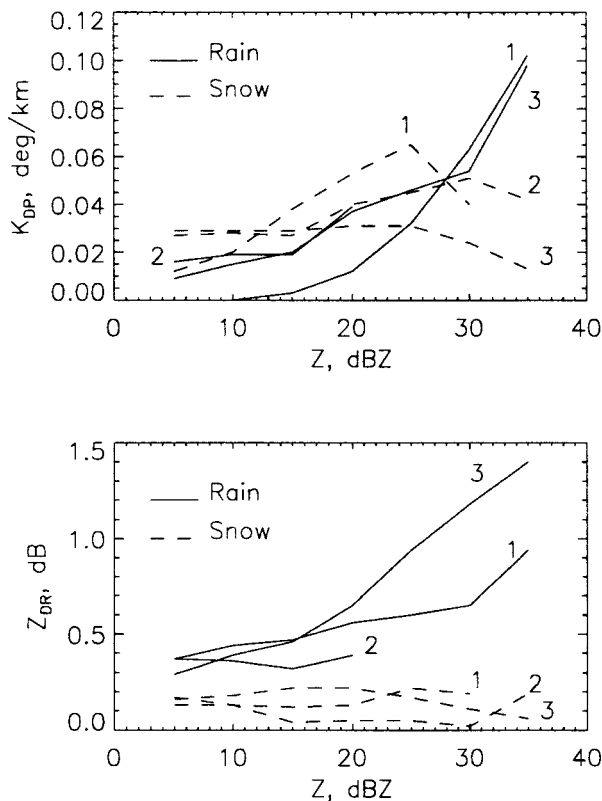


FIG. 3. (a) K_{DP} - Z and (b) Z_{DR} - Z dependencies for warm snow and rain in six different winterstorms. The designation of the curves is the same as in Fig. 2.

et al. 1991; Maekawa et al. 1993; Vivekanandan et al. 1994; Ryzhkov and Zrnica 1998). Melting snowflakes observed routinely at the bright band exhibit a positive peak in Z_{DR} at the bottom of the melting layer accompanied by a deep minimum of the cross-correlation coefficient ρ_{hv} (Zrnica et al. 1993). The latter one is usually low in the regions of mixed-phased hydrometeors. In the transition region, within the frontal boundary separating snow from rain, the melting zone can be vertically elongated (Stewart 1992), and it is natural to expect localized ρ_{hv} and Z_{DR} extrema in this region.

The objective of this study is to examine radar polarimetric signatures of snowfall and to contrast them with those of rainfall. The other major focus is on investigation of methods to recognize the rain-snow transition boundary. In pursuit of these objectives, use is made of polarimetric radar data that have been collected in several Oklahoma snowstorms with the Cimarron 10-cm-wavelength radar (Zahrai and Zrnica 1993).

2. General characteristics of snowstorms

Overall more than 10 snowstorms were observed during the period from December 1993 to March 1996 in Oklahoma. Six of these have been studied in greater detail because supporting meteorological information

(soundings, surface and synoptic data) was available. They are classified into two categories according to (a) environmental conditions and (b) distinct polarimetric signatures. The first class includes storms that occurred on 1 March 1995, 2 March 1995, and 1 February 1996 in air masses quite cold for Oklahoma with surface temperature below -5°C over the whole observational area. These "cold" snowstorms have, on the average, a lower radar reflectivity factor and larger K_{DP} and Z_{DR} due to abundance of small ice crystals. No large aggregated snowflakes were observed precipitating from the cold storms. The second class consists of storms that occurred on 8 March 1994, 5 January 1995, and 18 December 1995. These were associated with cold fronts that separated regions of rain from regions of snow in the radar coverage area, so that it was possible to follow the transition between snow and rain over a substantial time interval. The surface temperatures in the "warm" snowstorms were near or slightly below 0°C . These storms contained heavily aggregated snow and, as a result, had larger reflectivities and, on the average, lower K_{DP} and Z_{DR} .

Both classes of snowstorms have much in common. They reveal an increase of Z_{DR} and K_{DP} as well as a decrease of Z with height. Figure 1 shows typical average profiles of Z , Z_{DR} , and K_{DP} for the cold storm of 1 March 1995 and the warm storm of 8 March 1994. To obtain each of the profiles in Fig. 1 we have selected typical cells in the snowstorm region and computed mean profiles of three radar variables over an area defined by 5° in azimuth and 10 km in range. The increase of Z_{DR} and K_{DP} with height might be attributed to abundance of pristine oriented crystals aloft. At lower altitudes (i.e., higher temperatures) aggregation becomes active. Because aggregates have a lower density and are less elongated than pristine crystals, they produce smaller Z_{DR} and K_{DP} . In the case of warm snow, the maximal value of Z_{DR} is lower but the maximal values of Z and K_{DP} are higher than in the cold snow case. More efficient aggregation for the warm snow results in lower Z_{DR} . However, larger concentration of particles in the warm snow case leads to the larger Z and K_{DP} . Here K_{DP} has a peak of about $0.35^{\circ}\text{km}^{-1}$ at the height of 5 km and decreases farther up due to the drop of the concentration near the upper cloud boundary. However, Z_{DR} is not dependent on concentration and, therefore, grows monotonically with height (up to the very top of the cloud) in both cases due to reduction in the degree of aggregation.

3. Polarimetric characteristics of snow

In this section we examine the trends of K_{DP} and Z_{DR} with the variation of Z in snow. Generally in ice-bearing parts of clouds the values of specific differential phase and differential reflectivity are relatively large. The values of K_{DP} as large as $0.8^{\circ}\text{km}^{-1}$ and Z_{DR} up to 3 dB are often observed at a 10-cm wavelength in the zones

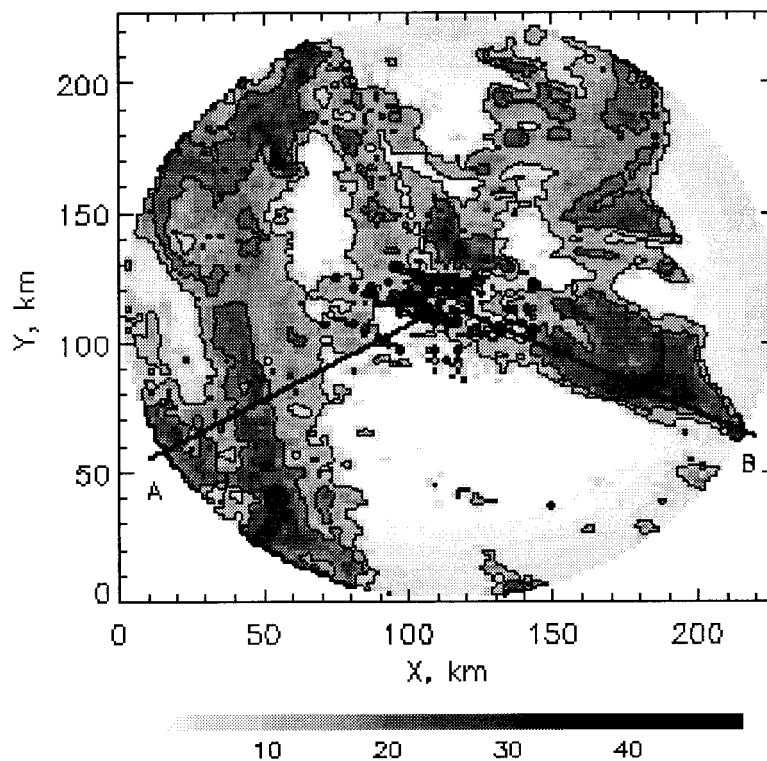


FIG. 4. Radar reflectivity at the elevation of 0.5° for the snowstorm of 5 Jan 1995. Time is 2127 UTC and the Z contours are drawn every 10 dBZ.

of low radar reflectivity (less than 20 dBZ) near the tops of summer and winter storms in Oklahoma; these are likely due to the dominance of small oriented pristine crystals at high altitudes. However, in snow near the ground aggregated crystals are usually the dominant type of hydrometeors, and both K_{DP} and Z_{DR} signatures are an order of magnitude weaker.

To establish the range of variation of polarimetric parameters in snow, we have examined K_{DP} , Z_{DR} , and Z data at the lowest elevation scan (usually 0.5°) for each snowstorm. After analyzing K_{DP} -Z and Z_{DR} -Z scattergrams for several successive scans we have determined the average trends of the polarimetric variables with the change of the radar reflectivity factor. Note that because the observed K_{DP} values are of the order of a few tenths or even hundredths of a degree per kilometer the estimates of K_{DP} were derived after filtering the differential phase data with a wide running average window over 48 consecutive range locations (Ryzhkov and Zrnica 1996). The sample spacing in range depends on the pulse repetition frequency and varies between 0.15 and 0.24 km and, therefore, the width of the averaging window is between 7.2 and 11.5 km. With this heavy filtering procedure, the standard deviation of the pointwise estimate of K_{DP} is about $0.05^\circ \text{ km}^{-1}$ in stratiform rain (Ryzhkov and Zrnica 1996). For snow the error is somewhat lower because the cross-correlation coefficient ρ_{hv} governing the accuracy of the differential phase

estimate is closer to unity than it is for rain. Additional spatial averaging further reduces the standard deviation of the K_{DP} estimate. Hence, the K_{DP} for a localized area (few tens of square kilometers) can be determined with the accuracy of about one-hundredth of a degree per kilometer. Differential reflectivity data were averaged over 24 successive range gates. The resulting error in Z_{DR} is about 0.10–0.15 dB (depending on the magnitude of the cross-correlation coefficient). Again, the areal average can be obtained with a higher accuracy.

The plots of average K_{DP} versus average Z and Z_{DR} versus Z for all six snowfalls (Fig. 2) indicate that K_{DP} varies between 0.01° and $0.08^\circ \text{ km}^{-1}$, whereas Z_{DR} is generally below 0.6 dB. For the cold storms the polarimetric parameters are larger. This increase is especially noticeable in the differential reflectivity data. Both polarimetric parameters reveal no pronounced trends with the change of the radar reflectivity factor for the range of examined $Z < 35$ dBZ. The K_{DP} curves show a slight increase within the reflectivity interval of 15–25 dBZ. We hypothesize that the opposite trends of the polarimetric variables and Z in the vertical profiles (Fig. 1) are largely due to the temperature change with altitude because that is a leading factor affecting crystal to aggregate conversion. For the data collected at the lowest levels, in air with relatively uniform temperature, there is no apparent dependence of Z_{DR} and K_{DP} on Z, as can be seen in Fig. 2.

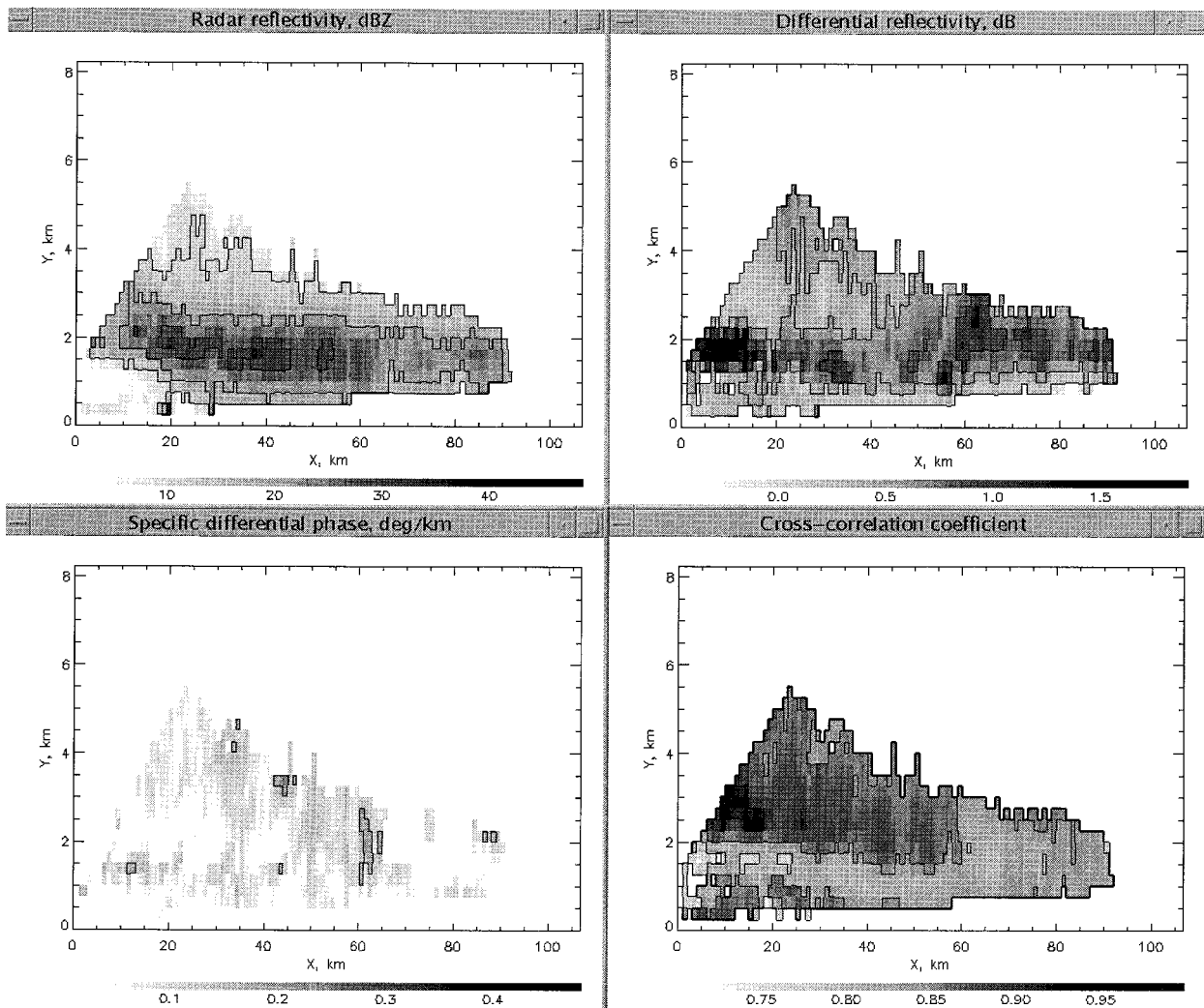


FIG. 5. Composite RHI plot of Z , Z_{DR} , K_{DP} , and ρ_{hv} in the azimuthal direction A , as shown in Fig. 4. Contours of Z are drawn every 10 dBZ starting at 10 dBZ, contours of Z_{DR} are drawn every 0.5 dB starting at 0 dB, contours of K_{DP} are drawn every $0.1^{\circ} \text{ km}^{-1}$ starting at $0.1^{\circ} \text{ km}^{-1}$, and contours of ρ_{hv} are drawn every 0.05 starting at 0.75.

4. Polarimetric discrimination between pure snow and pure rain

The rainy parts of the three warm storms have been analyzed in the same manner as the snowy parts. The location of the rainy areas in the mixed precipitation (warm) storms was determined using surface meteorological information. In Fig. 3 the average $K_{DP}(Z)$ and $Z_{DR}(Z)$ trends for rain are contrasted with those for the warm snow. It is hard to distinguish between the rain and the snow in the K_{DP} data if $Z < 30$ dBZ. However, discrimination using Z_{DR} is possible. We can qualify precipitation as snow if the differential reflectivity is lower than 0.2 dB and the reflectivity factor is below 35 dBZ. This signature is ambiguous with that caused by drizzle, where all liquid drops are practically spherical and the differential reflectivity is lower than in snow. Nevertheless, in all mixed-phase storms under

consideration the liquid fraction of hydrometeors had always enough nonspherical drops to produce Z_{DR} larger than that in snow. In rainfall, both K_{DP} and Z_{DR} rapidly increase with increasing Z .

Although the polarimetric contrasts between rainfall and snowfall near the ground are not very large, the difference in vertical structure is rather significant as examination of the 5 January 1995 case demonstrates. The reflectivity field at the elevation of 0.5° is shown in Fig. 4 for 2127 UTC. At that time heavy snowfall was associated with the azimuthal sector between 90° and 120° , which includes the Norman location where it was observed. At the same time, stratiform rain was observed at the ground in the western sector of the radar coverage area. The rainband was moving rapidly to the east, so the snowfall ultimately changed to rain over Norman.

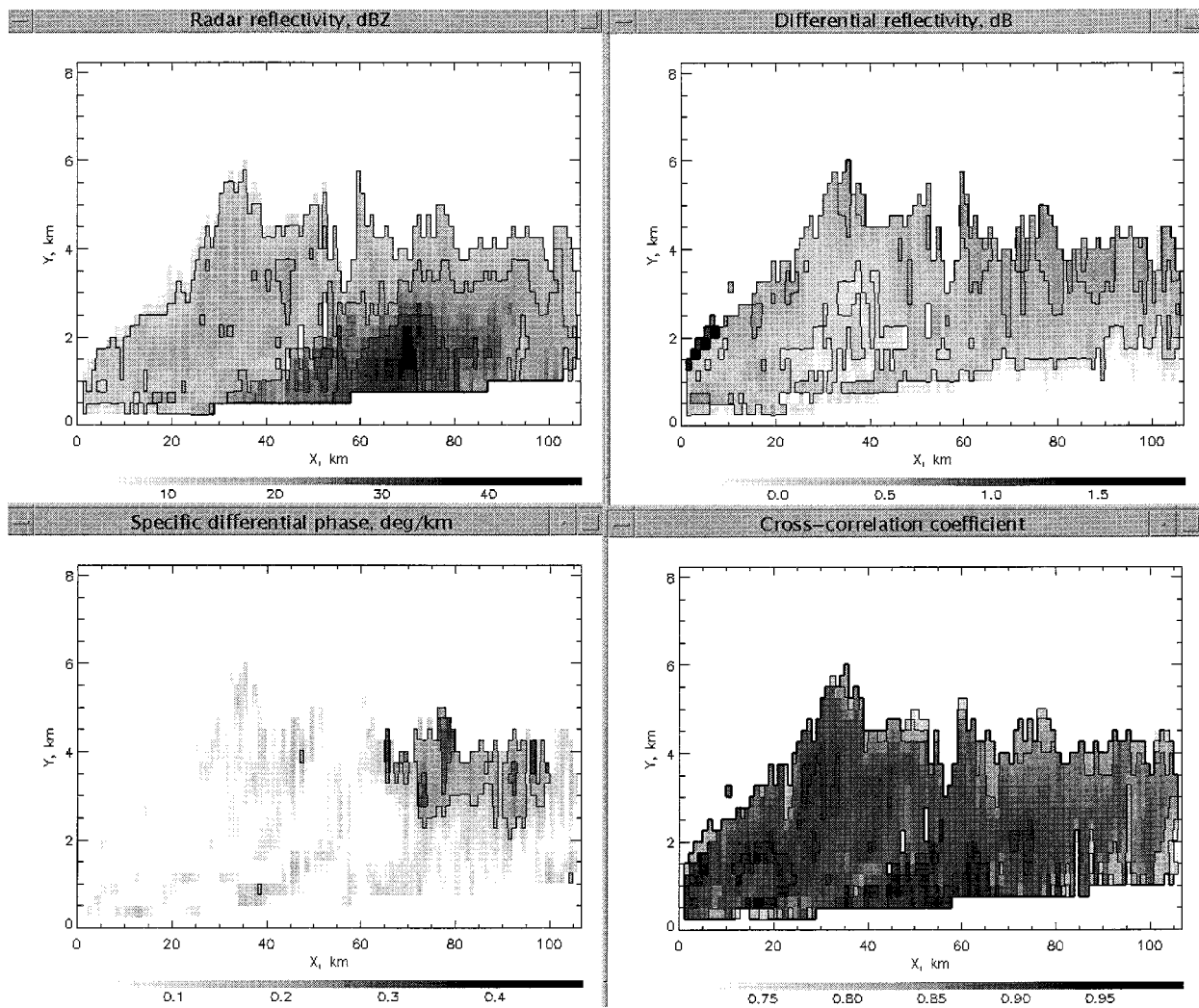


FIG. 6. Same as in Fig. 5 but in the azimuthal direction B, as shown in Fig. 4.

The composite range–height indicator (RHI) plots in Figs. 5 and 6 illustrate the difference in the vertical cross sections at azimuth A (rain in Fig. 4) and azimuth B (snow in Fig. 4). It is clear that one cannot distinguish between the snow and the rain using solely the reflectivity information either in the plan position indicator or the RHI mode. Neither can the specific differential phase provide discriminating clues in this particular case. But the fields of differential reflectivity and cross-correlation coefficient are highly informative. The melting layer is clearly marked by the Z_{DR} maximum and the ρ_{hv} minimum at the height between 1 and 2 km in the rain region (Fig. 5). In the area of snow, ρ_{hv} is quite constant, while Z_{DR} exhibits a steady increase with height (Fig. 6). The specific differential phase can be used to identify the region of high density ice at the height interval between 2.5 and 5 km (Fig. 6) where both K_{DP} and Z_{DR} reach their maxima.

5. Transition between rain and snow

In the case of 5 January 1995, there was a gap between rain- and snow bands in the radar reflectivity field; thus, the snow–rain line was nonexistent. In the other two warm snowstorm cases (8 March 1994 and 18 December 1995) the reflectivity fields had no breaks in the melting zone; this provided an opportunity to follow the change of the polarimetric variables in the transition region between snow and rain.

First, let us examine the 18 December 1995 storm. On that day, the cold front moved through central Oklahoma from west to east. A sequence of radar reflectivity factor images (on constant altitude surfaces, CAPPIS) at the height of 500 m is shown in Fig. 7. White solid and dashed lines indicate the locations of the 0° and 1°C isotherms, respectively, according to surface measurements. Surface observations in Norman (located at azimuth 141° and range 41 km from the radar) indicated

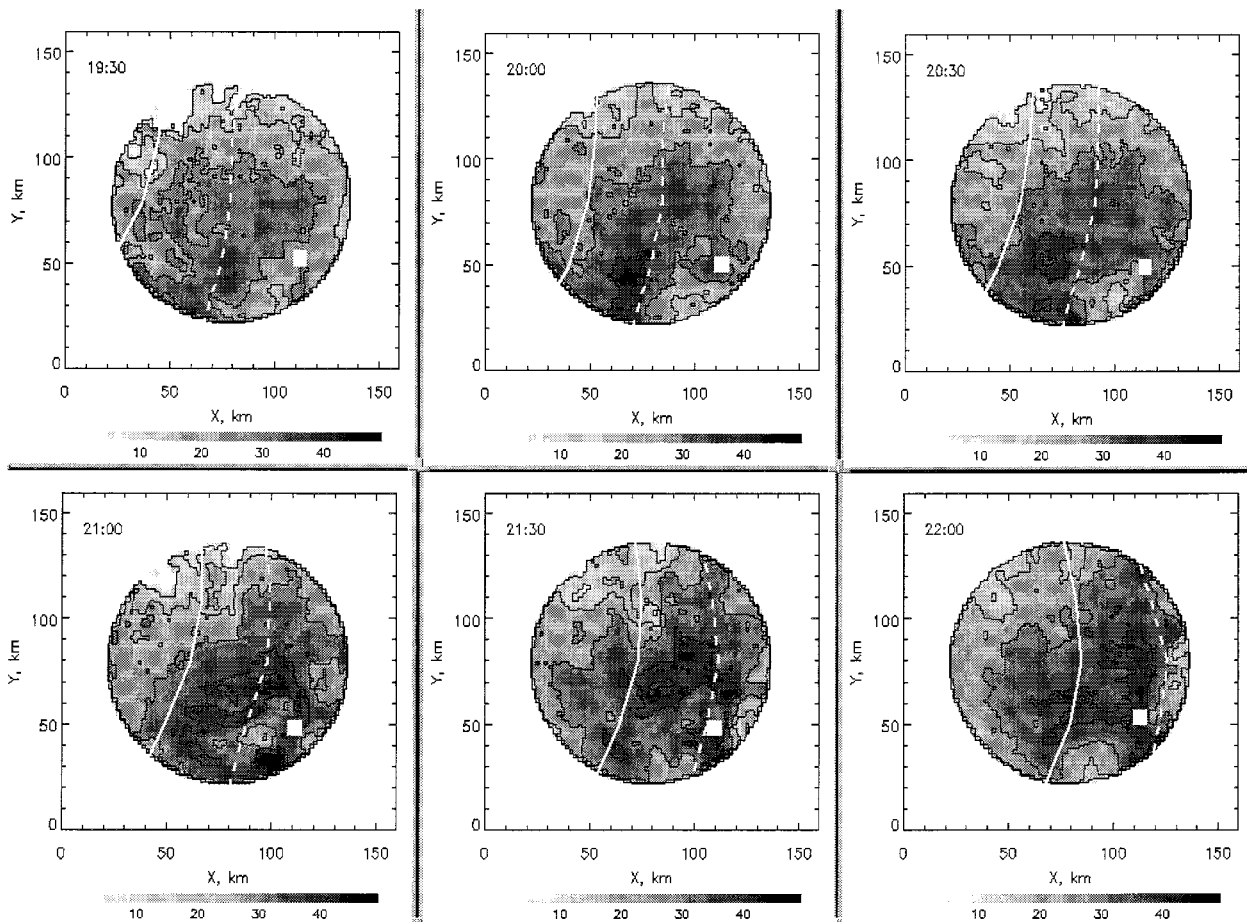


FIG. 7. Temporal sequence of the CAPPI images of Z at the height of 0.5 km for the storm of 18 Dec 1995. White solid and dashed lines depict the locations of 0° and 1°C isotherms on the ground, respectively. Contours of Z are drawn as in Fig. 4.

pure rain precipitation on the ground before 2140 UTC, when the first signs of snow mixed with rain appeared. Afterward, at 2210 UTC, very large snowflakes, 2–3 cm in diameter, were reported in Norman. Eventually this storm produced 4 in. of snow on the ground in the Norman area. As can be seen from Fig. 7, there is no clear indication of melting and snow–rain transition in the radar reflectivity field apart from some increase of Z primarily between the two isotherms.

At the same time, a very clear minimum in the cross-correlation coefficient associated with the 1°C isotherm is evident in the sequence of ρ_{hv} images (Fig. 8). Transformation of large melting snowflakes into raindrops is a plausible cause of the ρ_{hv} dip. This signature is similar to the one observed routinely in the horizontal melting layer of typical stratiform rain. In this particular case the “bright band” is vertically elongated and extends only for about 10 km in the horizontal direction, as can be seen from the composite RHI image represented in Fig. 9. Within this transition region ρ_{hv} drops below 0.5. The vertical extent of the minimum is about 1–1.5 km. It is very likely that this extent coincides with the vertically elongated region, or “isothermal layer” (Stewart

1992) that has a nearly constant slightly positive temperature. In a horizontally stratified atmosphere, the thickness of this layer does not exceed a few hundred meters (Stewart et al. 1984; Willis and Heymsfield 1989). Within the zone where the atmosphere is not horizontally stratified, the vertical extent of the isothermal layer can be significant and thus fill the radar beam. This might explain the observed extremely low values of the cross-correlation coefficient. Note that the ρ_{hv} minimum does not stretch along the 1°C isotherm everywhere but is localized in the limited area (Fig. 8) where the isothermal layer is supposedly deep enough to support generation of big snow aggregates. For example, Stewart (1992) showed that near 0°C layers, of the order of 1–3 km deep and up to 20 km across, are very favorable for generation of big aggregates. With a fall speed of 1 m s^{-1} , a particle could undergo enhanced aggregation for almost an hour before it strikes the surface. A well-pronounced cross-correlation signature exists in the transition region between snow and rain where large wet snow aggregates are generated.

Analysis of the sequence of differential reflectivity images shows that the zone of low Z_{DR} emerges directly

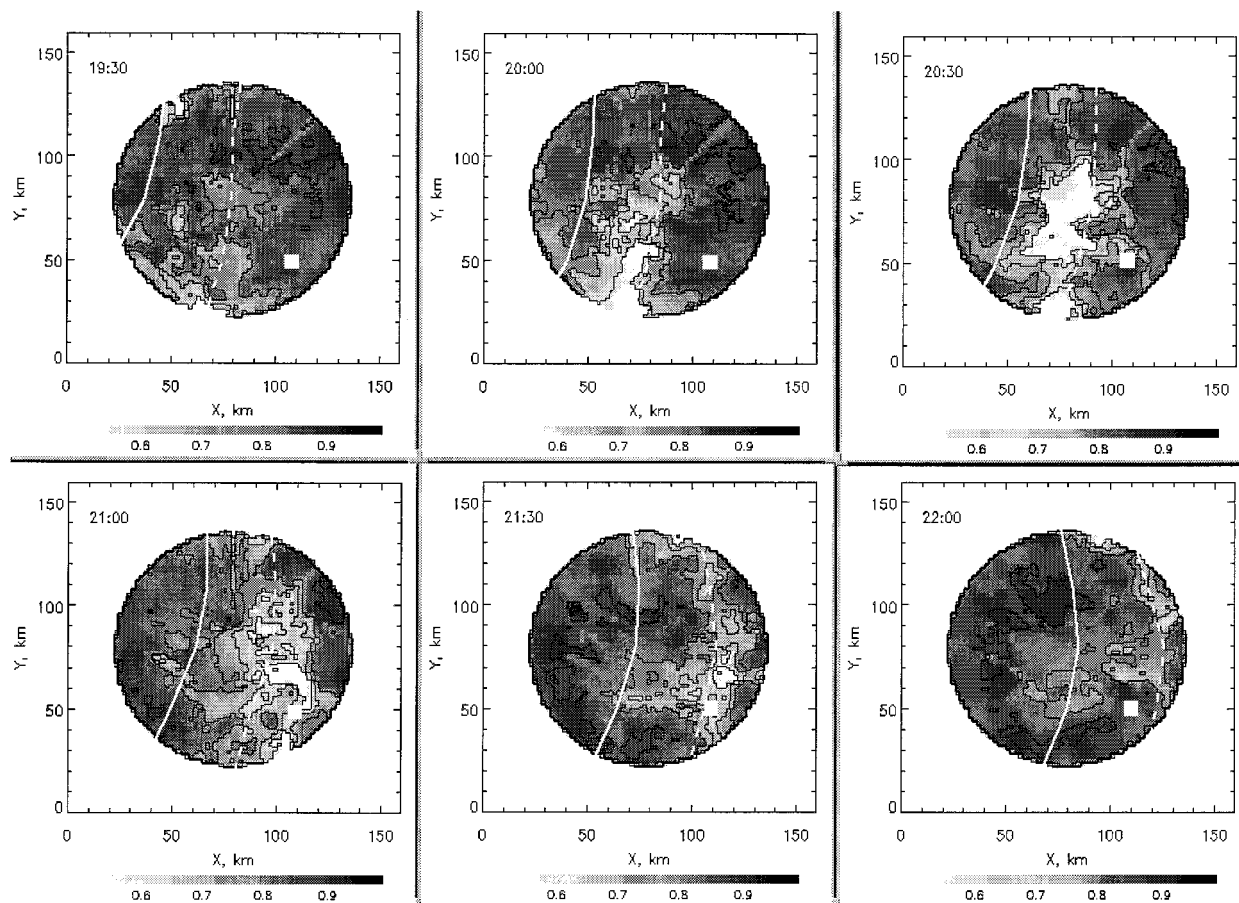


FIG. 8. Same as in Fig. 6 but for the cross-correlation coefficient.

behind the ρ_{hv} dip. A general decrease of Z_{DR} in the whole observational area as rain turns to snow is evident in Fig. 10. After 2130 UTC, the differential reflectivity is close to zero everywhere in the cold pool behind the 1°C isotherm. This confirms our major conclusion from Fig. 3 that for a given reflectivity factor, differential reflectivity is lower in snow than in rain. This contrast is especially well marked in the regions where large snowflakes are generated. It is evident from Fig. 10 that Z_{DR} is maximal at the leading edge of the cross-correlation dip (in rain precipitation), while Z is maximal at the trailing edge of the dip (in snow precipitation) where Z_{DR} drops to zero.

To follow the changes of the polarimetric variables we select a fixed $10\text{ km} \times 10\text{ km}$ area centered on Norman and plot in Fig. 11 temporal dependencies of Z , Z_{DR} , K_{DP} , and ρ_{hv} averaged over this area. The data are from the lowest elevation of 0.5° ; therefore, the corresponding height of the beam center for this area is between 400 and 500 m above the ground. As stated before, the change from pure rain to a rain–snow mixture occurred at 2140 UTC in Norman, which corresponds to time = 103 min on the x axis. That is the time within the abrupt transition of Z_{DR} from 2.3 to 0

dB. The cross-correlation coefficient reaches its minimum at time = 95 min, just before snow was first detected on the ground. The specific differential phase exhibits its maximum simultaneously with the ρ_{hv} minimum in the rain–snow mixture. At 2210 UTC (time = 133 min) when very large snowflakes were detected, radar reflectivity reached its maximum probably because the size of hydrometeors is largest, whereas Z_{DR} and K_{DP} are low since the bulk density of snowflakes is very low.

Interpretation of Fig. 11 can be facilitated by appealing to readers intuition and experience. Assume that the timescale in the figure is proportional to temperature (i.e., it is decreasing). Then replace the timescale on the x axis by a height scale (height decreases with temperature) and rotate the plot in Fig. 11 by 90° . Thus, obtained “vertical” profiles of the radar polarimetric parameters appear as typical profiles through the melting layer (Zrnica et al. 1993); the Z maximum is slightly above the Z_{DR} and ρ_{hv} extrema. Because the physics of melting is the same in the horizontal and vertical bright bands, it leads to analogous polarimetric signatures in both cases.

Analysis of the snowstorm of 8 March 1994 reveals

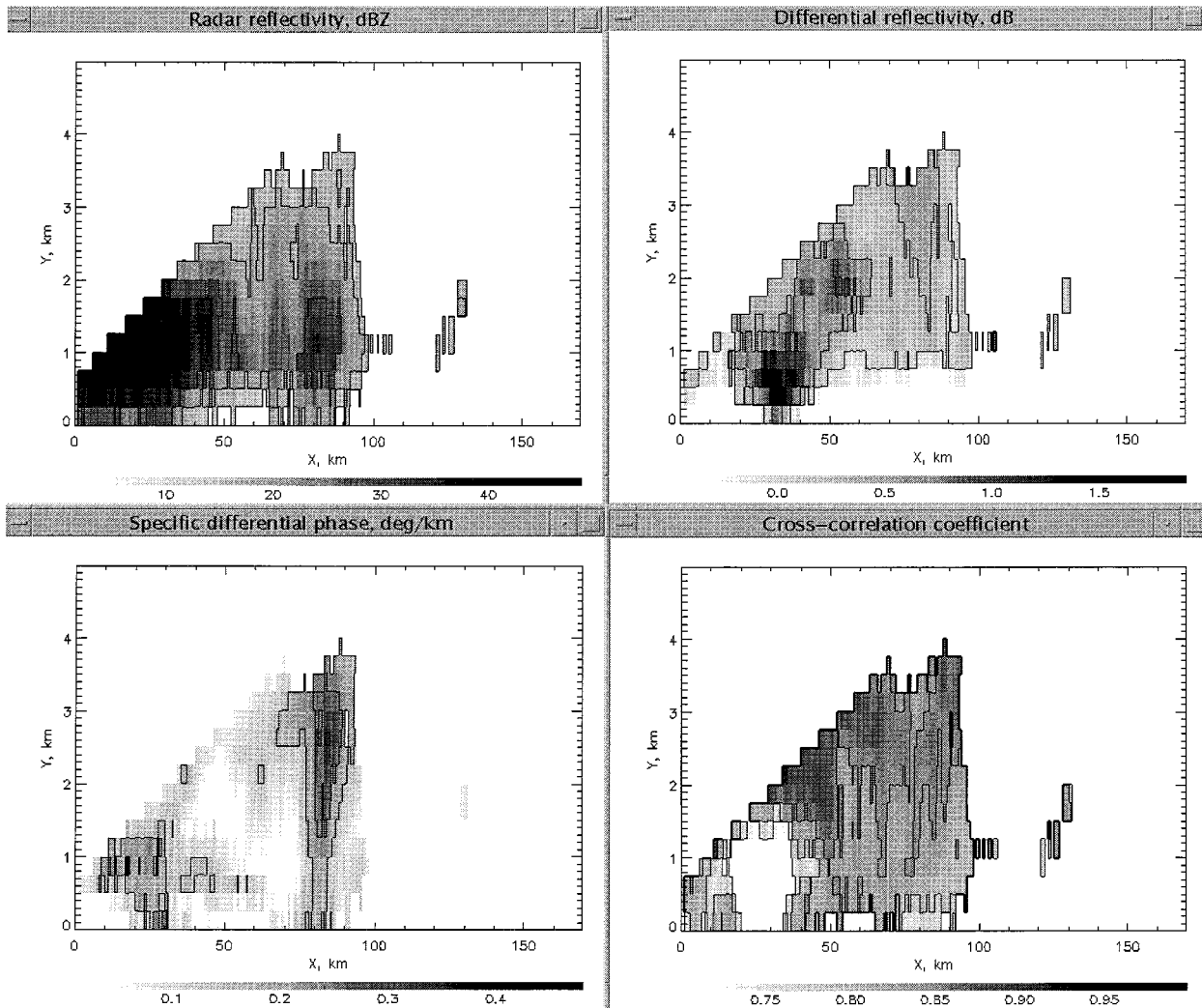


FIG. 9. Composite RHI plot of Z , Z_{DR} , K_{DP} , and ρ_{hv} in the azimuthal interval 110° – 115° for the storm of 18 Dec 1995. Time is 2127 UTC; the contours of the polarimetric variables are as in Fig. 5.

the same type of polarimetric pattern in the snow–rain transition zone as was observed for the storm of 18 December 1995. Shown in Fig. 12 is a composite CAPPI plot of Z , Z_{DR} , K_{DP} , and ρ_{hv} at the height level of 1 km. On that day a cold front was moving slowly southward. Again, the positions of the 0° and 1°C isotherms are indicated by the white solid and dashed lines, and the Norman location is shown as a triangle. The volume scan from which the radar data were taken started at 1912 UTC. According to surface observations, rain changed to snow in Norman at approximately 1900 UTC. The snow–rain transition zone is clearly outlined by a ρ_{hv} minimum, which again coincides with the 1°C isotherm. Both the radar reflectivity factor and the differential reflectivity reach their maxima directly to the south of the ρ_{hv} minimum region, at the very edge of the rainy sector of precipitation field. Note a wide area of a very low cross-correlation coefficient in the southwest corner of the ρ_{hv} image (Fig. 12) that is not confined

to the narrow transition region between snow and rain. This is an artifact of the ρ_{hv} data; the negative bias occurs in the region of high Doppler spectrum width σ_v associated with strong wind shear. A reason for the apparent reduction of ρ_{hv} in this regions is a combination of high spectrum width ($>5\text{ m s}^{-1}$) and quantization errors in our analog-to-digital converters to which cross-correlation estimates are sensitive. In the transition zone between snow and rain σ_v is moderate, so we consider ρ_{hv} estimates reliable in this area. This was concluded after analyzing ρ_{hv} , σ_v , and signal-to-noise ratio (SNR) data of this and other storms collected with the Cimarron radar. Similar analysis of ρ_{hv} and σ_v data obtained by the National Center for Atmospheric Research (NCAR) S-POL polarimetric radar revealed no visible reduction of ρ_{hv} at high σ_v , provided that the SNR is over 20 dB.

A composite of RHIs of four polarimetric variables is represented in Fig. 13; the azimuthal direction is 142° and the time is 1912 UTC. In this case the cross-cor-

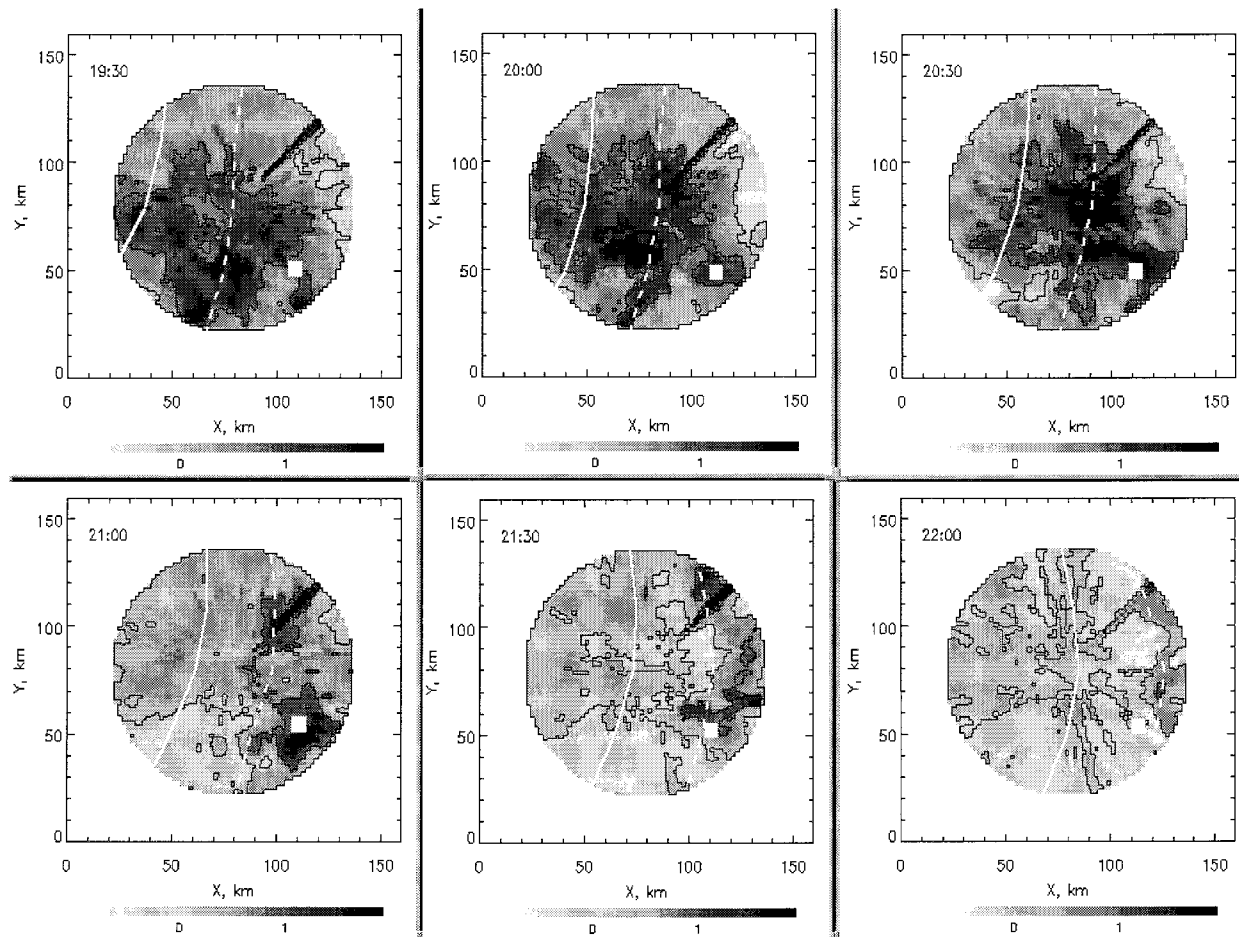


FIG. 10. Same as in Fig. 6 but the field is for differential reflectivity.

relation minimum is elevated; that is, it does not reach the ground but is contained within the altitude interval between 0.5 and 1.5 km. Similar to the previous case, the Z_{DR} maximum is situated adjacent to the ρ_{hv} dip in the rainy region of precipitation.

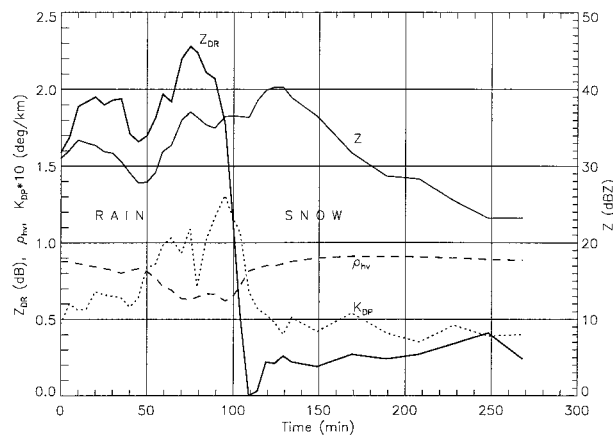


FIG. 11. Temporal dependence of Z , Z_{DR} , K_{DP} , and ρ_{hv} at the Norman location for the storm of 18 December 1995.

6. Conclusions

Polarimetric signatures of precipitation in six Oklahoma snowstorms have been examined using the 10-cm-wavelength Cimarron polarimetric radar. Specific differential phase K_{DP} , differential reflectivity Z_{DR} , cross-correlation coefficient ρ_{hv} , as well as radar reflectivity factor Z were available for analysis.

It was established that in pure snow average values of K_{DP} and Z_{DR} do not follow a systematic trend with change of the radar reflectivity factor if $Z < 35$ dBZ and do not exceed $0.08^\circ \text{ km}^{-1}$ and 0.6 dB, respectively. In “cold” snowstorms (surface temperature is below -5°C) both polarimetric variables are higher than in “warm” snowstorms (i.e., near the snow–rain boundary) due to abundance of heavily aggregated snow in the latter type of storms. In ice-bearing regions aloft in winter or summer clouds, the polarimetric parameters K_{DP} and Z_{DR} can be an order of magnitude higher than those in snow precipitation near the ground.

Contrary to what happens in snow, both K_{DP} and Z_{DR} grow rapidly in rain as the reflectivity factor increases. As far as warm snow is considered a Z_{DR} threshold of

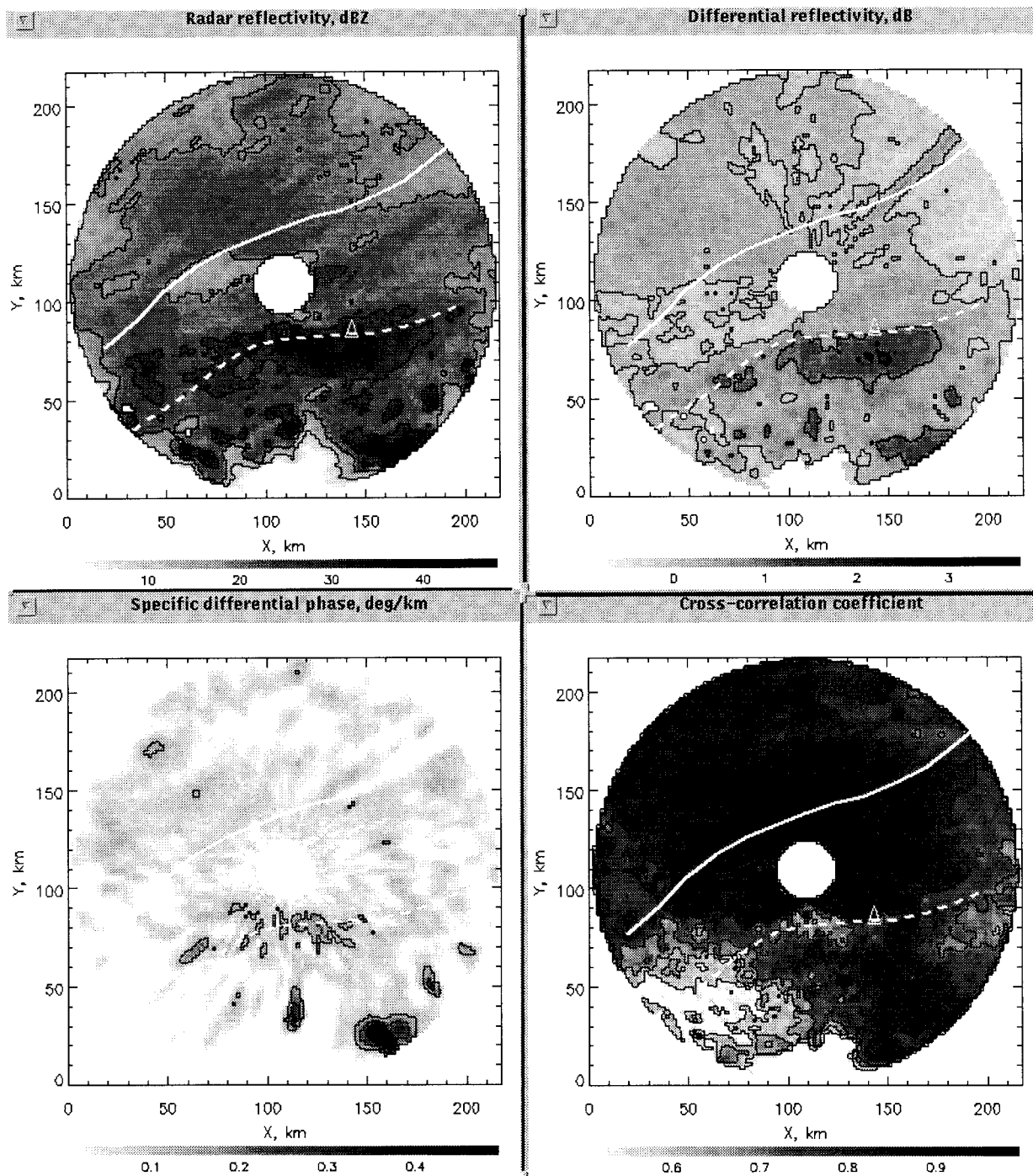


FIG. 12. The composite CAPPi image of Z , Z_{DR} , K_{DP} , and ρ_{hv} at the height of 1.0 km for the storm of 8 Mar 1994. White solid and dashed lines depict the locations of 0° and 1°C isotherms, respectively. The contours of Z_{DR} are drawn every 1 dB starting at 0 dB, contours of K_{DP} are drawn every $0.1^{\circ}\text{ km}^{-1}$ starting at $0.1^{\circ}\text{ km}^{-1}$, and contours of ρ_{hv} are drawn every 0.1 starting at 0.6. The contours of polarimetric variables are as in Fig. 5.

0.2 dB can be used to discriminate between pure rain and pure snow for reflectivities below 35 dBZ. Precipitation is classified as snow if the average Z_{DR} is less than 0.2 dB for $Z < 35$ dBZ. A pronounced ρ_{hv} minimum and a Z_{DR} maximum more effectively delineate the

bright band than does the reflectivity factor and, thus, are good discernible features for discrimination between snow and rain precipitation.

A localized deep minimum of the cross-correlation coefficient delineates the transition boundary between

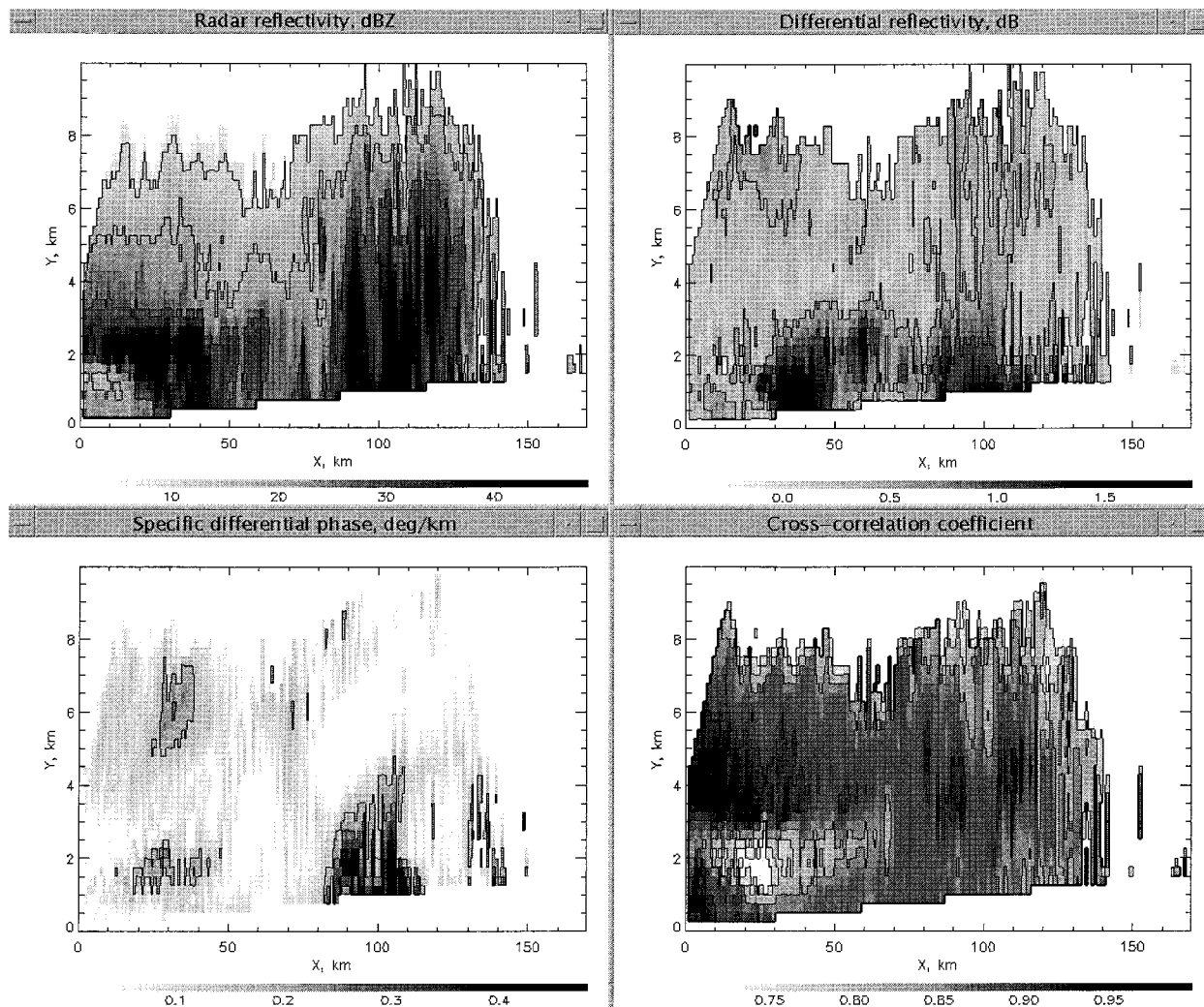


FIG. 13. Composite RHI plot of Z , Z_{DR} , K_{DP} , and ρ_{hv} in the azimuthal interval 140° – 145° for the storm of 8 Mar 1994. Time is 1912 UTC, and the contours of polarimetric variables are as in Fig. 5.

snow and rain in the horizontal plane if sufficiently large snowflakes are generated in the transition area. Otherwise, the Z_{DR} increase in the melting region can be used to localize the position of the snow–rain boundary. The position of the 1°C isotherm near the surface coincides with the actual transition region between snow and rain and is marked by a clear polarimetric signature of the melting aggregates.

Acknowledgments. Mike Schmidt and Richard Wahnkinney have maintained and calibrated the Cimarron radar. The authors are grateful to Ed Brandes from NCAR for the sample of data collected by the S-POL radar that helped clarify our concerns about the cross-correlation estimator performance. We acknowledge Brent Gordon's assistance in getting supporting surface and sounding data for several days of radar observations.

REFERENCES

- Aydin, K., T. A. Seliga, and V. Balaji, 1986: Remote sensing of hail with a dual linear polarization radar. *J. Climate Appl. Meteor.*, **25**, 1475–1484.
- Balakrishnan, N., and D. S. Zrníc, 1990: Estimation of rain and hail rates in mixed-phase precipitation. *J. Atmos. Sci.*, **47**, 565–583.
- Brown, P., and P. Francis, 1995: Improved measurements of the ice water content in cirrus using a total-water probe. *J. Atmos. Oceanic Technol.*, **12**, 410–414.
- Fabry, F., and I. Zawadzki, 1995: Long-term observations of the melting layer of precipitation and their interpretation. *J. Atmos. Sci.*, **52**, 838–851.
- Gunn, K. L. S., and J. S. Marshall, 1958: The distribution with size of aggregate snowflakes. *J. Meteor.*, **15**, 452–461.
- Hall, M., J. Goddard, and S. Cherry, 1984: Identification of hydrometeors and other targets by dual-polarization radar. *Radio Sci.*, **19**, 132–140.
- Leitao, M. J., and P. A. Watson, 1984: Application of dual linearly polarized radar data to prediction of microwave path attenuation. *Radio Sci.*, **19**, 209–221.
- Maekawa, Y., S. Fukao, Y. Sono, and F. Yoshino, 1993: Distribution

- of ice particles in wintertime thunderclouds detected by a C band dual polarization radar: A case study. *J. Geophys. Res.*, **98**, 16 613–16 622.
- Martner, B. E., J. Snyder, R. Zamora, G. Byrd, T. Nizol, and P. Joe, 1993: A remote-sensing view of a freezing-rain storm. *Mon. Wea. Rev.*, **121**, 2562–2577.
- Meischner, P., V. N. Bringi, M. Hagen, and H. Holler, 1991: Multi-parameter radar characterization of a melting layer compared with in situ measurements. Preprints, *25th Int. Conf. on Radar Meteorology*, Paris, France, Amer. Meteor. Soc., 721–724.
- Ryzhkov, A. V., and D. S. Zrnic, 1996: Assessment of rainfall measurement that uses specific differential phase. *J. Appl. Meteor.*, **35**, 2080–2090.
- , and ———, 1998: Polarimetric method for ice water content determination. *J. Appl. Meteor.*, **37**, 125–134.
- Stewart, R. E., 1992: Precipitation types in the transition region of winter storms. *Bull. Amer. Meteor. Soc.*, **73**, 287–296.
- , J. D. Marwitz, J. C. Pace, and R. E. Carbone, 1984: Characteristics through the melting layer of stratiform clouds. *J. Atmos. Sci.*, **41**, 3227–3237.
- Vivekanandan, J., V. N. Bringi, M. Hagen, and P. Meischner, 1994: Polarimetric radar studies of atmospheric ice particles. *IEEE Trans. Geosci. Remote Sens.*, **32**, 1–10.
- Willis, T. W., and A. J. Heymsfield, 1989: Structure of the melting layer in mesoscale convective system stratiform precipitation. *J. Atmos. Sci.*, **46**, 2008–2025.
- Zahrai, A., and D. S. Zrnic, 1993: The 10-cm wavelength polarimetric weather radar at NOAA's National Severe Storms Laboratory. *J. Atmos. Oceanic Technol.*, **10**, 649–662.
- Zrnic, D. S., N. Balakrishnan, C. Ziegler, V. Bringi, K. Aydin, and T. Matejka, 1993: Polarimetric signatures in the stratiform region of a mesoscale convective system. *J. Appl. Meteor.*, **32**, 678–693.